THE JOURNAL OF PHYSICAL CHEMISTRY Letters

Perspective

Cite This: J. Phys. Chem. Lett. 2019, 10, 4476−4483

pubs.acs.org/JPCL

Titration of Aerosol pH through Droplet Coalescence

Ellen M. Coddens, Kyle J. Angle, and Vicki H. Grassian*

Department of Chemistry and Biochemistry, University of California San Diego, La Jolla, California 92093, United States

Supporting Information

ABSTRACT: The pH of aqueous aerosols, as well as cloud and fog droplets, has an important influence on the chemistry that takes place within these unique microenvironments. Utilizing conjugate acid/base pairs to infer pH changes, we investigate, for the first time, changes in aerosol pH upon coalescence. In particular, we show that the pH within individual aqueous aerosols that are ∼8 μm in diameter can be titrated via droplet coalescence in an aerosol optical tweezer. Using sulfate/bisulfate and carbonate/bicarbonate as model systems, the pH of trapped aerosols is determined before and after introduction of smaller aerosols containing a strong acid. The pH change upon coalescence with the smaller, acidic aerosol is calculated using specific ion interaction theory. Furthermore, we show that the pH of an individual aerosol can be altered along a fairly wide range of pH values, paving the way for future studies requiring rigorous pH control of an aqueous aerosol.

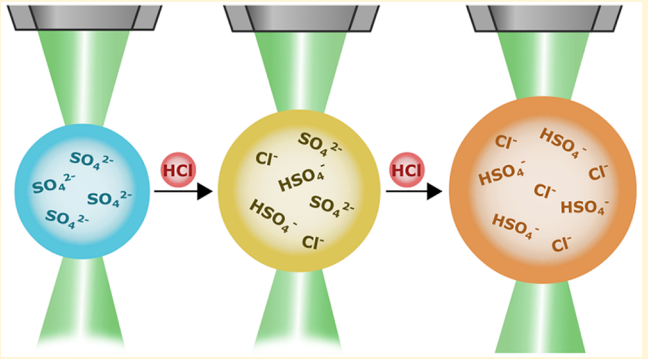

Acidity is a key factor in aerosol chemistry, as well as in the chemistry that occurs in cloud and fog droplets. The microenvironment within an individual aerosol can be very different from that of a bulk solution, and therefore, it is important that pH within individual aerosols be measured *and* controlled. Many atmospheric multiphase chemical processes are pH-dependent, including transition-metal-catalyzed oxidation processes and secondary organic aerosol formation.[1−5] For inorganic and organic acids, molecular and ionic speciation of acid/base conjugate pairs depends on pH, and for metals, such as iron, solubility and speciation are highly pH-dependent. Therefore, it is extremely important to take pH into account when studying aqueous aerosol chemistry.[6−15]

Although cloudwater is generally acidic with a pH around 5, more alkaline cloud pH values around 7 have been reported, and very low pH aqueous environments within aerosols (pH less than 3) have been proposed as well.[16−22] This indicates that droplets in the atmosphere, whether as aqueous aerosols or in cloud and fog waters, are highly variable in terms of pH. Furthermore, the chemistry *within* the microenvironment of a droplet and at the *surface* of the droplet can be different from that of a bulk solution.[23−26]

Given that pH is a key factor in aerosol, cloud, and fog chemistry, there are very few direct measurements of aerosol pH. Most methods for determining aerosol pH in the past have used indirect proxy methods. The main proxy methods used to estimate aerosol acidity include the ion balance method, the molar ratio method, thermodynamic equilibrium models, and phase partitioning of ammonia.[27] All of these methods provide valuable information, yet each has limitations that prevent their widespread application. Therefore, there is a need for better methods for directly determining aerosol pH.[28] Recently, Ault and Dutcher, along with their co-workers, have made great strides in this regard. In several seminal papers, it was shown that the pH for substrate-deposited aerosol particles can be directly determined using Raman microspectroscopy (vide infra).[29−31] In more recent work, colorimetric image processing was used to determine the pH of aerosol particles that were directly deposited onto pH paper.[32]

> All of the methods used to estimate aerosol acidity provide valuable information, yet each has limitations that prevent widespread application.

Table 1 summarizes these different direct and indirect methods for determining aerosol pH and includes the main advantages and disadvantages of each method, along with some key points.[29−41] The indirect methods were previously discussed in detail in a review by Hennigan et al.[27]

In addition to various methods of measuring aerosol pH, there are also multiple approaches to calculating solution pH based on chemical equilibria. One widely used approach is the Henderson−Hasselbalch (H−H) equation (eq 1)

$$\mathrm{pH} = \mathrm{p}K_a + \log \frac{[\mathrm{A}^-]}{[\mathrm{HA}]} \quad (1)$$

Received: March 16, 2019
Accepted: July 12, 2019
Published: July 12, 2019

DOI: 10.1021/acs.jpclett.9b00757
J. Phys. Chem. Lett. 2019, 10, 4476−4483

Table 1. Summary of Direct and Indirect Methods for Determining Aerosol pH

Method	Advantages	Disadvantages	Refs
Direct Methods			
inorganic or electrochemical measurement of filter extracts	few empirical constants needed; some methods portable; useful to observe trends of changes in bulk properties	requires time-intensive sample filtering; poor resolution; prone to sampling artifacts such as failure to denuder and remove alkaline particles or interaction of particles with denuder coating	27,38−40
individual particle measurement via spectroscopy	nondestructive; few assumptions required; precise information on size and refractive index simultaneously obtained	useful ion pair (e.g., SO_4^{2-}/HSO_4^-) must be present at detectable concentrations; works for limited size range; works best when ion pair peaks are of similar intensity	29−31
aerosol deposition onto pH paper	particles need not be predried or filtered; ambient results can be obtained in ∼2 h	some indicators require correction for systematic bias; each indicator most useful in the middle of its range; need to account for species absorbing in the visible	32
fluorescent probe microscopy	highly sensitive; can monitor liquid−liquid phase separation	pH range limited to ∼2 units	41
surface-enhanced Raman spectroscopy	information on pH distribution within a substrate deposited aerosol can be obtained	there is discussion that this method may measure the concentration of H^+ rather than activity	35,37
Indirect Methods			
ion balance	simple and useful for inorganic systems	organic compounds complicate results; model failed to correlate with known results of some field campaigns	27
molar ratio	adaptable to various ion composition profiles and absolute concentrations	high uncertainty; disagrees with established models	27
thermodynamic equilibrium models (e.g., E-AIM, ISORROPIA, AIOM-FAC)	widely applicable; can use either total aerosol + gas content ("forward") or individual component ("reverse") concentrations as input	various models substantially disagree; models diverge when ammonia is dilute; "reverse" mode highly sensitive to minor ionic measurement errors; low liquid water content of aerosols can result in low precision; many ignore organics; requires equilibrium	27,33,34
phase partitioning	recommended for high accuracy	requires system to have reached equilibrium, which is often untrue, especially for large aerosols; sensitive to uncertainty in ammonia concentration and variations in ionic strength	36

where pH is calculated through knowledge of the pK_a and the ratio of the concentrations of acid, [HA], and its conjugate base, $[A^-]$.[42] The pH derived from the Henderson−Hasselbalch equation is simply from the definition of the equilibrium constant, K_a, in logarithmic form. However, eq 1 is applicable to a limited range of solution conditions and does not take into account nonideal behavior and ion activity. This results in a breakdown of the H−H equation for relatively strong acids or bases as well as for systems where activity coefficients cannot be neglected.[43,44] The Debye−Hückel theory (DHT) and specific ion interaction theory (SIT) can be used to calculate ion activities. Both of these approaches more accurately determine pH by taking into account deviations from ideal solution behavior by calculating activity coefficients for strong electrolyte solutions.[42,45,46]

DHT was recently applied to substrate-deposited aerosol particles. Aerosol pH was determined using experimental data from Raman spectroscopy of conjugate acid/base pairs along with extended DHT.[29−31] In this method, activity coefficients, γ_i, for species i are determined by the extended Debye−Hückel equation (eq 2)

$$-\log \gamma_i = \frac{Az_i^2\sqrt{I}}{1 + aB\sqrt{I}} = D \tag{2}$$

where A and B are constants characteristic of the solvent (water) and a is the effective diameter of the ion in solution. I is the ionic strength of the solution

$$I = \frac{1}{2}\sum c_i z_i^2 \tag{3}$$

which is calculated from the concentration (molarity), c_i, and charge, z_i, of each ion. The activity, a_i, can be related to the dissociation constant, K_a

$$K_a = \frac{a_{H^+} \times a_{A^-}}{a_{HA}} = \frac{([H^+]\gamma_{H^+})([A^-]\gamma_{A^-})}{[HA]\gamma_{HA}} \tag{4}$$

for a system in equilibrium. The pH of the substrate-deposited particle pH can be calculated

$$pH = -\log(a_{H^+}) = -\log([H^+]\gamma_{H^+}) \tag{5}$$

after iteratively solving for γ_{H^+} and a_{H^+}.

The Debye−Hückel method works best for low electrolyte concentrations and is most accurate for aqueous solutions with ionic strengths ≤ 0.1 m.[45,47] Additionally, one of the major assumptions of the Debye−Hückel model is that the interactions between ions occur only through long-range electrostatic interactions. However, in more concentrated electrolyte solutions, shorter-range specific ion−ion interactions need to be considered as well.[46,48] Thus, in some cases, DHT fails to account for interactions between ions based on their identity and therefore can poorly predict H^+ activity.

The SIT model provides an alternative method for predicting activity coefficients (eq 6)

$$\log \gamma_i = -z_i^2 D + \sum_k \varepsilon(i, k, I) m_k \tag{6}$$

by taking the interactions of specific ions in solution into account using ion interaction coefficients

$$\varepsilon = \varepsilon_1 + \varepsilon_2 \times \log(I) \tag{7}$$

where ε is the interaction coefficient of species i with species k and the summation is extended over all species present at the molality m_k and is dependent on the ionic strength of the solution.[46,49,50] In eq 6, D is the Debye−Hückel term described by eq 2. The ion interaction coefficient, which depends on ionic strength, empirically describes the specific short-range interactions between species i and k in solution. The coefficients are determined from electrochemical measurements, and the coefficients of many common species are available in the literature.[46,51] A table of coefficients and constants used in DHT and SIT calculations can be found in the Supporting Information (Table S1).

DOI: 10.1021/acs.jpclett.9b00757
J. Phys. Chem. Lett. 2019, 10, 4476−4483

Given the wide range of experimental and computational methods available for determining pH, it is essential that each method accurately reflects the activity of H^+. In the current study, we examine the validity of calculating the pH of individual aerosols by combining Raman measurements with H−H, DHT, and SIT. Aerosols produced are not passed through a diffusion dryer or impacted onto a substrate, therefore removing the need to consider any effects due to drying or possible substrate effects. We also examine the extent to which this method can be used to calculate the changing pH of an aerosol upon titration as manipulation of aerosol pH would be essential to studying environmental reactions at atmospherically relevant pH values.

Here, pH is calculated for both bulk solutions and aerosol using DHT and SIT by first determining calibration curves of concentration versus integrated peak area from Raman spectra of one of the conjugate acid/base pairs (e.g., sulfate in the bisulfate/sulfate system and carbonate in the bicarbonate/carbonate system). For bulk solutions, a confocal Raman spectrometer is used to create the calibration curves for aqueous solutions. For an aerosol (∼8 μm diameter), an aerosol optical tweezer combined with a cavity enhanced Raman spectrometer is used to determine the Raman intensity as a function of concentration. Calibration curves for sulfate and carbonate are given in Figures S1 and S2 in the Supporting Information. The conjugate ion concentrations are calculated under the assumption that the total sulfur concentration is constant for sulfate/bisulfate, or in the case of carbonate/bicarbonate the total carbon is constant, and that the concentration in the trapped aerosol is the same as in the bulk solution. Sulfate and bisulfate concentrations (or carbonate and bicarbonate concentrations) and ionic strength are then used to determine activity coefficients, and ultimately pH, by iteratively solving eqs 2−7. For experiments in which aerosol pH is titrated via droplet coalescence with a more acidic aerosol (vide infra), changes in ionic strength with acid dosing are taken into account. In comparison, when calculating pH using the H−H method, the ratio of sulfate to bisulfate is determined by comparing the integrated peak area of the sulfate and bisulfate vibrational bands from the Raman spectra.

Before applying these calculations to trapped aerosols, we first investigated bulk solutions near the same concentrations and pH that are used for aerosol experiments and calculated pH using the three methods discussed above—H−H, DHT, and SIT—to determine which one provides the most accurate calculation from known bulk solutions (see additional information in the Supporting Information). The results are summarized in Figure 1, where the dashed line represents the case where bulk measured pH is equal to the calculated pH. By comparing all three methods, it can be seen that the SIT method is closest in agreement with the dashed line, indicating that pH determined via the SIT method is in greatest agreement with the experimentally measured values compared to the DHT or H−H methods for these solutions. Therefore, SIT is used for determining aerosol pH.

Using bulk aqueous solutions of known pH, aerosols were generated using an ultrasonic nebulizer, and the pH of the trapped aerosol was calculated, as done above for bulk solutions, but with the calibration curve obtained for aerosol as shown in Figure S1b. Figure 2 compares the bulk measured pH to the calculated particle pH for trapped sulfate and carbonate aerosols where the dashed line represents the case where the measured bulk pH is equal to that of the calculated particle pH. From this plot, it can be seen that the majority of the calculated pH values for the trapped aerosol lie below the 1:1 line, indicating that there is acidification during the formation of the aerosol and trapping process. Ault and Dutcher, as well as others, have observed a similar trend in acidification during the aerosolization process, although it should be noted that in these studies, the aerosol was sent through a diffusion dryer leading to a decrease in pH.[29−31,52] Additionally, following the method described by Ault and co-workers,[32] pH was determined using colorimetric analysis by

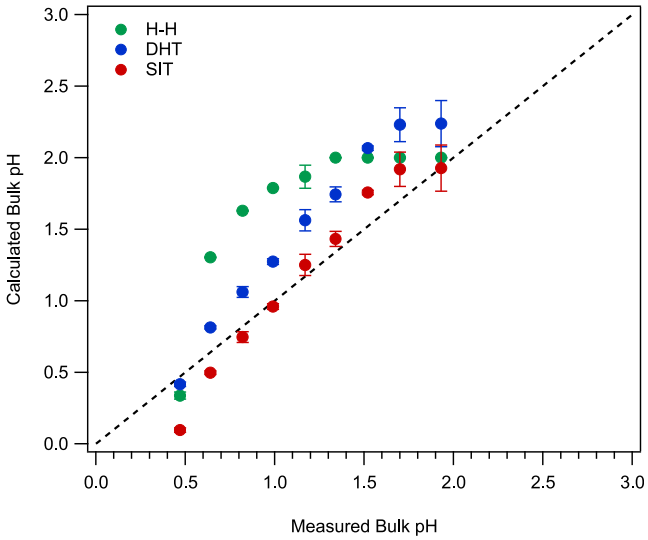

Figure 1. Comparison of experimentally measured bulk solution pH to calculated bulk solution pH using H−H equation (green), DHT (blue), or SIT (red) methods. Calculated pH values are determined using the equations provided in the main text and sulfate concentrations obtained from the calibration curve shown in Figure S1a. The dashed line represents the 1:1 line where bulk measured pH is equal to that of calculated pH.

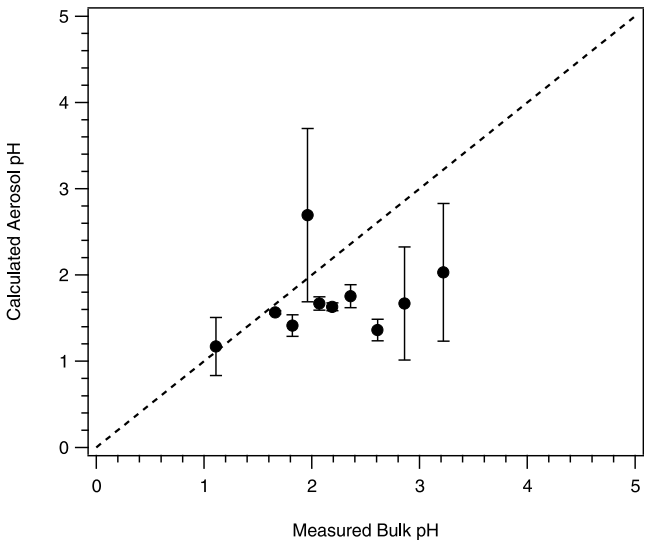

Figure 2. Comparison of measured bulk pH to calculated aerosol pH using the SIT method for trapped sulfate aerosol. Calculated pH values are determined by eqs 2−7 where sulfate concentration is obtained using the calibration curve from Figure S1b. The dashed line represents the 1:1 line where measured bulk pH is equal to the calculated aerosol pH. It can be seen that in most cases, the aerosol pH is more acidic than the bulk pH.

DOI: 10.1021/acs.jpclett.9b00757
J. Phys. Chem. Lett. 2019, 10, 4476−4483

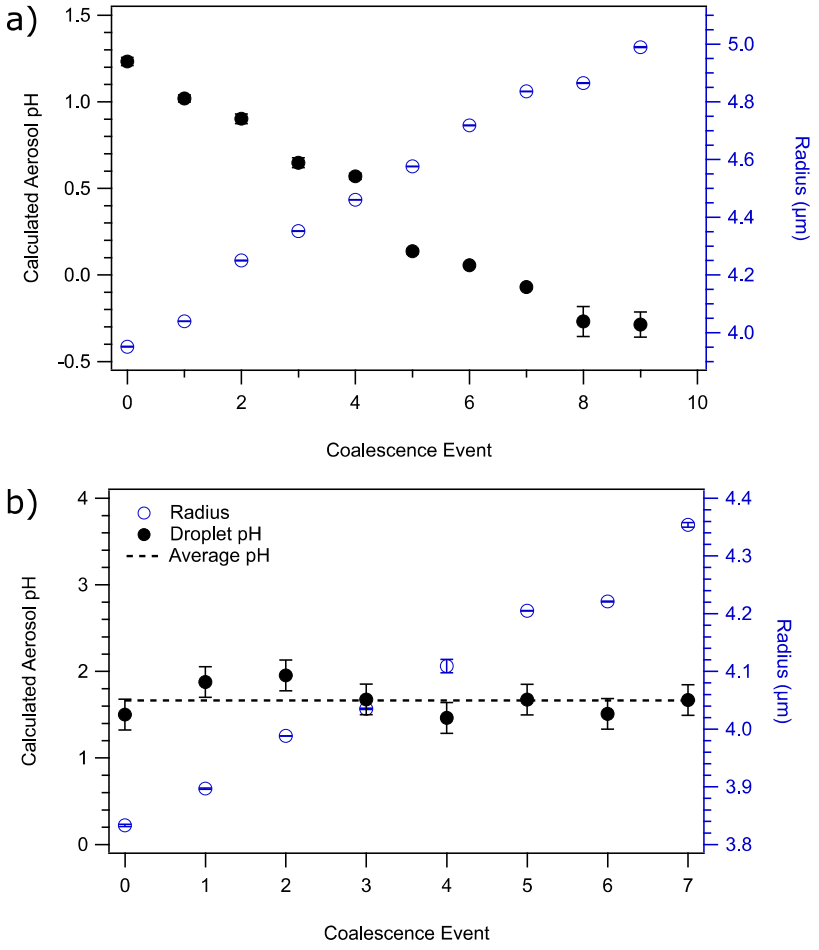

Figure 3. (a) Calculated aerosol pH (closed, black circles) and radii (open, blue circles) of a trapped sulfate aerosol coalesced with a smaller acidic aerosol prepared from a 1 M HCl solution. Following each coalescence event, there is a decrease in aerosol pH and corresponding increase in aerosol size as coalescence proceeds from coalescence event 0 to 9, where 0 is the initial aerosol before any coalescence. (b) Calculated aerosol pH and radii of a trapped sulfate aerosol following coalescence with water of the same pH (2.1), indicating that the initial aerosol pH does not change, as expected for this control experiment. The dashed line is the average calculated aerosol pH over the entire range of coalescence events (see images of a coalescence event in Figure S4).

directly impacting aerosols generated by the nebulizer onto pH paper, the results of which are summarized in Figure S3 and confirm acidification upon nebulization (see the Supporting Information for more detail). Overall, these results show that the bulk pH and aerosol pH are not the same and can differ depending on how the aerosol is prepared from a bulk solution for laboratory studies.

Once trapped, aerosol pH can be changed and further probed. This is done by introducing more acidic aerosol containing HCl into the trapping chamber while monitoring the Raman spectra before and after each coalescence event. A detailed description of the trapping and coalescence methods can be found in the Supporting Information. For each trapped aerosol, the pH is calculated before and after each coalescence event. However, it should be noted that the current method does not take into account equilibration with the surrounding gas phase and volatilization which may be important in other systems. For example, in the ammonium sulfate or ammonium nitrate systems, ammonia diffusion and partitioning from the particle to gas phase should be considered.

Calculated aerosol pH as a function of coalescence event for a sulfate aerosol repeatedly coalesced with a more acidic, smaller aerosol is shown in Figure 3a. As radius increases, the calculated pH decreases with each consecutive coalescence event. Additionally, this change in pH can be seen spectroscopically by examining the ratio of conjugate acid/base pairs. For example, Figure S5 depicts the change in peak area ratios for sulfate/bisulfate as a trapped sulfate aerosol is titrated with a smaller, more acidic aerosol. With each coalescence event, the $\nu_1(SO_4^{2-})$ band decreases while the $\nu(HSO_4^-)$ band increases, corresponding to a shift in equilibrium and a decrease in pH. This decrease in pH upon coalescence demonstrates the ability to change or control the pH of a trapped aerosol via coalescence with a smaller, acidic aerosol.

Control experiments were also done and are shown in Figure 3b. In this plot, the change in calculated pH and radii of a trapped sulfate aerosol coalesced with a solution of the same pH, instead of a more acidic aerosol, are shown. Although the radius increases with each consecutive coalescence, there is little variation in calculated pH with each coalescence event, indicating that, at a constant relative humidity, the aerosol grows because of coalescence but no significant change in aerosol pH is observed. This can also be seen by examining the symmetric stretch of the sulfate vibrational mode $\nu_1(SO_4^{2-})$ at 985 cm^{-1} in the Raman spectra. The integrated peak area of the $\nu_1(SO_4^{2-})$ clearly decreases with each coalescence event when coalesced with an acidic solution (Figure S6a) as

DOI: 10.1021/acs.jpclett.9b00757
J. Phys. Chem. Lett. 2019, 10, 4476−4483

compared to the minor changes in the vibrational band when coalesced with a solution of the same pH (Figure S6b, control experiment).

Similar experiments were performed to examine the influence that concentration of the smaller, acidic aerosol has on the change in pH of the initially trapped aerosol. Figure 4

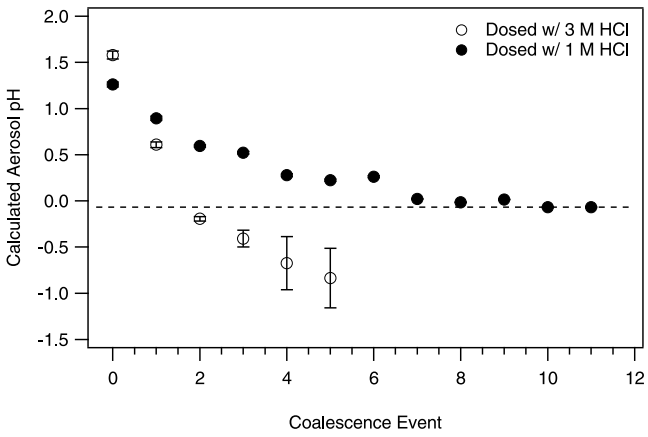

Figure 4. Calculated pH of trapped sulfate aerosol coalesced with smaller acidic aerosols prepared from 1 M (closed circles) or 3 M (open circles) hydrochloric acid solutions. Calculated pH is shown as a function of the number of coalescence events where 0 is the calculated pH of the trapped aerosol prior to coalescence. The dashed line represents the value at which pH levels off for coalescence experiments with 1 M HCl.

shows the calculated pH of sulfate aerosol, trapped from the same initial bulk solution, titrated with 1 or 3 M HCl. With both concentrations of acid, as coalescence progresses the calculated pH of the aerosol decreases because the aerosol is further acidified with each coalescence event. In Figure 4, the dashed line represents the pH value for which the calculated aerosol pH begins to level off after multiple coalescence events. As expected, this pH value is near the pH of the bulk acid sample (pH 0 and −0.48 for 1 and 3 M HCl, respectively). This is because as the number of coalescences increases, the mole fraction of HCl within the aerosol increases and approaches the pH of the more acidic aerosol. This observation is important to note as it shows how the SIT method can be used to accurately determine aerosol pH.

Additionally, the rate at which the aerosol acidifies as it is titrated increases when coalescing with smaller, acidic aerosol prepared from 3 M HCl solutions compared to 1 M HCl solutions, and fewer coalescence events are required to cause the same decrease in aerosol pH when using the more concentrated acid. For example, as seen in Figure 4, only one coalescence event is required to reach a pH of approximately 0.5 with 3 M HCl, whereas two coalescence events are needed to reach the same pH with 1 M HCl. However, it should be noted that the change in pH with each coalescence is not consistent, which could be due to multiple reasons. First, the pH scale is logarithmic; as a result, if each coalescence added the same number of H^+ ions, the change in pH would be larger for cases where the starting pH is higher. Therefore, the *change* in pH is expected to diminish over time as the concentration of H^+ continues to increase. Second, the variation in amount of change in pH per coalescence event may be attributed to the inconsistency in the size of the final aerosol following coalescence. With the current nebulization method, there is little control over the exact size of the smaller, acidic aerosol (i.e., the incoming aerosol to be coalesced with the aerosol that is within the optical trap). The nebulizer used in these experiments produces a range of aerosol sizes with a reported mass median aerodynamic diameter of ca. 5 μm. Although there is currently little control of the size of the incoming aerosol, the size can be estimated by calculating the change in radius of the trapped aerosol after coalescence, for this experiment, the average incoming acidic aerosol was 0.1 μm in radius. To obtain better control of size, additional nebulization methods should be considered. Nonetheless, the pH of a trapped aerosol can be changed and titrated via coalescence with a more acidic aerosol.

To investigate if this method for determining and controlling aerosol pH through coalescence is applicable to other chemical systems, the same method was applied to the carbonate/bicarbonate system. Using the concentration calibration curve determined via AOT cavity enhanced Raman spectroscopy (Figure S2), the pH of a trapped carbonate aerosol can be determined from a bulk solution (see Figure S7 in the Supporting Information) and following titration with a smaller, acidic aerosol as summarized in Figure 5. Because of the

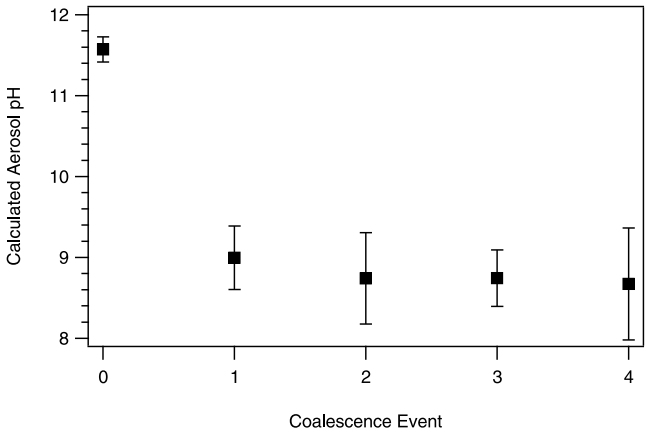

Figure 5. Calculated pH of a trapped carbonate aerosol, from a bulk solution with a measured pH of 12.4, coalesced with a smaller particle from a 1 M HCl solution. Calculated pH is shown as a function of the number of coalescence events, where 0 is the calculated pH of the trapped aerosol prior to acid coalescence.

difference in chemical properties of sulfate and carbonate, titration was limited to the pH region near the pK_a (specifically, pK_{a2} = 10.33[53]) to avoid the formation and release of carbon dioxide, which occurs at lower pH. As shown in Figure 5, there is a decrease in pH with each coalescence event and a leveling off of pH after multiple coalescences, similar to the case with sulfate. A larger error is associated with the carbonate system, as compared to sulfate, because of the changes in intensity in the Raman spectra. In the case of sulfate, as the aerosol underwent coalescence with a smaller acidic aerosol, the $\nu_1(SO_4^{2-})$ vibrational mode remained prominent, whereas for carbonate, the $\nu_1(CO_3^{2-})$ vibrational mode began to diminish with each coalescence, therefore resulting in greater uncertainty associated with the peak-fitting process. This error can be minimized by using a higher concentration of carbonate, therefore making the carbonate vibrational mode more pronounced. Additionally, it should be noted that the calculated initial particle pH is lower than that

DOI: 10.1021/acs.jpclett.9b00757
J. Phys. Chem. Lett. 2019, 10, 4476−4483

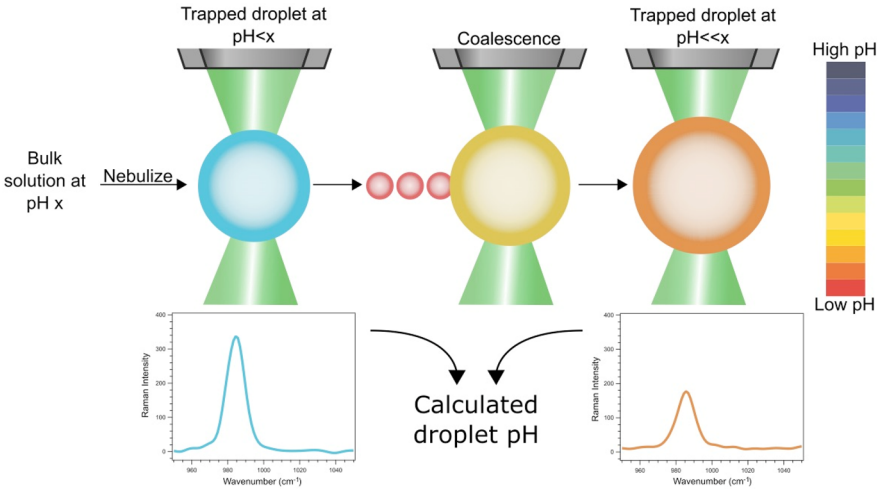

Figure 6. Schematic of the aerosol-trapping process from bulk solutions of pH *x*. The initial pH of the aerosol is less than that of the bulk solution. The aerosol pH can be changed through coalescence with another aerosol at a different pH. Raman spectra from the trapped particle are used in conjunction with calibration curves to determine concentration and ultimately calculate the following aerosol pH.

of the bulk solution, again demonstrating the acidification effect on aerosolization of a bulk solution.

From this work we have shown that control of aerosol pH is attainable through coalescence with acid and can be applied to multiple chemical systems. Figure 6 summarizes the experimental technique used here to calculate and control aerosol pH. Additionally, future experiments include coalescing a trapped aerosol with a smaller more basic aerosol to show that aerosol pH can also be increased through coalescence. With both acid and base coalescence, aerosol titration over a range of pH values is possible. In addition to control over aerosol pH, this technique also allows for control over the gaseous medium and relative humidity surrounding the trapped aerosol. This control over aerosol pH and its environment would allow studies of individual aerosols within dynamic environments, similar to those in the atmosphere, to be mimicked and probed in the laboratory. These laboratory-based single-aerosol studies provide valuable information, such as chemical kinetics of reactions within individual aerosols or elucidation of surface effects by comparing bulk phase chemical reactions and kinetics to those in the aerosol phase, which can be used in atmospheric chemistry models to more accurately predict and simulate aerosol chemistry. It is also worth noting that the method described in the current studies is capable of measuring pH of a single trapped aerosol but cannot differentiate between the surface or bulk of the aerosol. Therefore, future experiments designed to probe acidity at the aerosol surface would require surface-sensitive methods such as SFG and/or recently developed methods using mass spectrometry.[54−56]

These results also underscore the high ionic strength environments and the nonideal behavior within an aerosol. SIT calculations of pH have been provided to take this into account, and it was shown that SIT calculations for high ionic strength bulk solutions are in good agreement with the measured bulk pH. Using these SIT calculations, we can predict aerosol pH limits following repeated coalescence with smaller acidic aerosols to the pH of the acidic aerosol. There is a need for similar confirmation be done for other direct pH measurement in order to verify the reliability of the method to measure environmental samples. Overall, the results presented here provide evidence for a method to calculate aerosol pH and change aerosol pH via droplet coalescence that will allow examination of pH-dependent speciation, pH-dependent reactions, and other pH effects within a single aerosol that can be used in laboratory studies to better understand the physical chemistry of atmospherically relevant aerosols.

The results presented here provide evidence for a method to calculate aerosol pH and change aerosol pH via droplet coalescence that will allow examination of pH-dependent speciation, pH-dependent reactions, and other pH effects within a single aerosol that can be used in laboratory studies to better understand the physical chemistry of atmospherically relevant aerosols.

■ ASSOCIATED CONTENT

Supporting Information

The Supporting Information is available free of charge on the ACS Publications website at DOI: 10.1021/acs.jpclett.9b00757.

Details of the experimental methods, constants and table of ion interaction coefficients used in DHT and SIT calculations, Raman spectra and calibration curves for sulfate and carbonate, comparison of bulk and aerosol pH determined by deposition onto pH paper, images of a trapped aerosol undergoing coalescence, spectra of trapped aerosols coalesced with an acidic aerosol and aerosol of the same pH, and comparison of measured pH to calculated pH for carbonate (PDF)

■ AUTHOR INFORMATION

Corresponding Author

*E-mail: vhgrassian@ucsd.edu.

DOI: 10.1021/acs.jpclett.9b00757
J. Phys. Chem. Lett. 2019, 10, 4476−4483

ORCID

Ellen M. Coddens: 0000-0002-4441-1536
Kyle J. Angle: 0000-0001-7018-6718
Vicki H. Grassian: 0000-0001-5052-0045

Notes

The authors declare no competing financial interest.

■ ACKNOWLEDGMENTS

This material is based upon work supported by the National Science Foundation under Grant AGS1702488. Any opinions, findings, and conclusions or recommendations expressed in this material are those of the authors and do not necessarily reflect the views of the National Science Foundation. The authors thank Professor Cari Dutcher for thoughtful comments.

■ REFERENCES

(1) Huang, L.; Cochran, R. E.; Coddens, E. M.; Grassian, V. H. Formation of Organosulfur Compounds through Transition Metal Ion-Catalyzed Aqueous Phase Reactions. *Environ. Sci. Technol. Lett.* **2018**, *5*, 315−321.

(2) Surratt, J. D.; Gómez-González, Y.; Chan, A. W. H.; Vermeylen, R.; Shahgholi, M.; Kleindienst, T. E.; Edney, E. O.; Offenberg, J. H.; Lewandowski, M.; Jaoui, M.; et al. Organosulfate Formation in Biogenic Secondary Organic Aerosol. *J. Phys. Chem. A* **2008**, *112*, 8345−8378.

(3) Limbeck, A.; Kulmala, M.; Puxbaum, H. Secondary Organic Aerosol Formation in the Atmosphere via Heterogeneous Reaction of Gaseous Isoprene on Acidic Particles. *Geophys. Res. Lett.* **2003**, *30*, DOI: 10.1029/2003GL017738.

(4) Jang, M.; Czoschke, N. M.; Lee, S.; Kamens, R. M. Heterogeneous Atmospheric Aerosol Production by Acid-Catalyzed Particle-Phase Reactions. *Science* **2002**, *298*, 814−817.

(5) Wong, J. P. S.; Lee, A. K. Y.; Abbatt, J. P. D. Impacts of Sulfate Seed Acidity and Water Content on Isoprene Secondary Organic Aerosol Formation. *Environ. Sci. Technol.* **2015**, *49*, 13215−13221.

(6) Cwiertny, D. M.; Baltrusaitis, J.; Hunter, G. J.; Laskin, A.; Scherer, M. M.; Grassian, V. H. Characterization and Acid-Mobilization Study of Iron-Containing Mineral Dust Source Materials. *J. Geophys. Res. Atmos.* **2008**, *113*, D05202.

(7) Fu, H.; Cwiertny, D. M.; Carmichael, G. R.; Scherer, M. M.; Grassian, V. H. Photoreductive Dissolution of Fe-Containing Mineral Dust Particles in Acidic Media. *J. Geophys. Res.* **2010**, *115*, D11304.

(8) Gankanda, A.; Coddens, E. M.; Zhang, Y.; Cwiertny, D. M.; Grassian, V. H. Sulfate Formation Catalyzed by Coal Fly Ash, Mineral Dust and Iron (III) Oxide: Variable Influence of Temperature and Light. *Environ. Sci. Process. Impacts* **2016**, *18*, 1484−1491.

(9) Mackie, D. S.; Boyd, P. W.; Hunter, K. A.; McTainsh, G. H. Simulating the Cloud Processing of Iron in Australian Dust: pH and Dust Concentration. *Geophys. Res. Lett.* **2005**, *32*, L06809.

(10) Pruppacher, H. R.; Jaenicke, R. The Processing of Water Vapor and Aerosols by Atmospheric Clouds, a Global Estimate. *Atmos. Res.* **1995**, *38*, 283−295.

(11) Shi, Z.; Bonneville, S.; Krom, M. D.; Carslaw, K. S.; Jickells, T. D.; Baker, A. R.; Benning, L. G. Iron Dissolution Kinetics of Mineral Dust at Low pH during Simulated Atmospheric Processing. *Atmos. Chem. Phys.* **2011**, *11*, 995−1007.

(12) Solmon, F.; Chuang, P. Y.; Meskhidze, N.; Chen, Y. Acidic Processing of Mineral Dust Iron by Anthropogenic Compounds over the North Pacific Ocean. *J. Geophys. Res.* **2009**, *114*, D02305.

(13) Spokes, L. J.; Jickells, T. D.; Lim, B. Solubilisation of Aerosol Trace Metals by Cloud Processing: A Laboratory Study. *Geochim. Cosmochim. Acta* **1994**, *58*, 3281−3287.

(14) Spokes, L. J.; Jickells, T. D. Factors Controlling the Solubility of Aerosol Trace Metals in the Atmosphere and on Mixing into Seawater. *Aquat. Geochem.* **1996**, *1*, 355−374.

(15) Zhuang, G.; Yi, Z.; Duce, R. A.; Brown, P. R. Link between Iron and Sulphur Cycles Suggested by Detection of Fe(n) in Remote Marine Aerosols. *Nature* **1992**, *355*, 537−539.

(16) Khemani, L. T.; Momin, G. A.; Naik, M. S.; Prakasa Rao, P. S.; Safai, P. D.; Murty, A. S. R. Influence of Alkaline Particulates on pH of Cloud and Rain Water in India. *Atmos. Environ.* **1987**, *21*, 1137−1145.

(17) Weathers, K. C.; Likens, G. E.; Bormann, F. H.; Eaton, J. S.; Bowden, W. B.; Andersen, J. L.; Cass, D. A.; Galloway, J. N.; Keene, W. C.; Kimball, K. D.; et al. A Regional Acidic Cloud/Fog Water Event in the Eastern United States. *Nature* **1986**, *319*, 657−658.

(18) Pöschl, U. Atmospheric Aerosols: Composition, Transformation, Climate and Health Effects. *Angew. Chem., Int. Ed.* **2005**, *44*, 7520−7540.

(19) Zhang, X. Y.; Wang, Y. Q.; Niu, T.; Zhang, X. C.; Gong, S. L.; Zhang, Y. M.; Sun, J. Y. Atmospheric Aerosol Compositions in China: Spatial/Temporal Variability, Chemical Signature, Regional Haze Distribution and Comparisons with Global Aerosols. *Atmos. Chem. Phys.* **2012**, *12*, 779−799.

(20) Xue, J.; Yuan, Z.; Griffith, S. M.; Yu, X.; Lau, A. K. H.; Yu, J. Z. Sulfate Formation Enhanced by a Cocktail of High NOx, SO2, Particulate Matter, and Droplet pH during Haze-Fog Events in Megacities in China: An Observation-Based Modeling Investigation. *Environ. Sci. Technol.* **2016**, *50*, 7325−7334.

(21) Seinfeld, J. H.; Pandis, S. N. *Atmospheric Chemistry and Physics: From Air Pollution to Climate Change*, 2nd ed.; John Wiley & Sons, Inc.: Hoboken, NJ, 2006.

(22) Ding, J.; Zhao, P.; Su, J.; Dong, Q.; Du, X. Aerosol pH and Its Influencing Factors in Beijing. *Atmos. Chem. Phys. Discuss.* **2018**, *19*, 7939.

(23) Wellen, B. A.; Lach, E. A.; Allen, H. C Surface pKa of Octanoic, Nonanoic, and Decanoic Fatty Acids at the Air-Water Interface: Applications to Atmospheric Aerosol Chemistry. *Phys. Chem. Chem. Phys.* **2017**, *19*, 26551−26558.

(24) Zhang, T.; Brantley, S. L.; Verreault, D.; Dhankani, R.; Corcelli, S. A.; Allen, H. C. Effect of pH and Salt on Surface pKa of Phosphatidic Acid Monolayers. *Langmuir* **2018**, *34*, 530−539.

(25) Eugene, A. J.; Pillar, E. A.; Colussi, A. J.; Guzman, M. I. Enhanced Acidity of Acetic and Pyruvic Acids on the Surface of Water. *Langmuir* **2018**, *34*, 9307−9313.

(26) Lin, P.-C.; Wu, Z.-H.; Chen, M.-S.; Li, Y.-L.; Chen, W.-R.; Huang, T.-P.; Lee, Y.-Y.; Wang, C. C. Interfacial Solvation and Surface pH of Phenol and Dihydroxybenzene Aqueous Nanoaerosols Unveiled by Aerosol VUV Photoelectron Spectroscopy. *J. Phys. Chem. B* **2017**, *121*, 1054−1067.

(27) Hennigan, C. J.; Izumi, J.; Sullivan, A. P.; Weber, R. J.; Nenes, A. A Critical Evaluation of Proxy Methods Used to Estimate the Acidity of Atmospheric Particles. *Atmos. Chem. Phys.* **2015**, *15*, 2775−2790.

(28) Keene, W. C.; Sander, R.; Pszenny, A. A.; Vogt, R.; Crutzen, P. J.; Galloway, J. N. Aerosol pH in the Marine Boundary Layer: A Review and Model Evaluation. *J. Aerosol Sci.* **1998**, *29*, 339−356.

(29) Rindelaub, J. D.; Craig, R. L.; Nandy, L.; Bondy, A. L.; Dutcher, C. S.; Shepson, P. B.; Ault, A. P. Direct Measurement of pH in Individual Particles via Raman Microspectroscopy and Variation in Acidity with Relative Humidity. *J. Phys. Chem. A* **2016**, *120*, 911−917.

(30) Craig, R. L.; Nandy, L.; Axson, J. L.; Dutcher, C. S.; Ault, A. P. Spectroscopic Determination of Aerosol pH from Acid−Base Equilibria in Inorganic, Organic, and Mixed Systems. *J. Phys. Chem. A* **2017**, *121*, 5690−5699.

(31) Craig, R. L.; Ault, A. P. Aerosol Acidity: Direct Measurement from a Spectroscopic Method. In *Multiphase Environmental Chemistry in the Atmosphere*; Hunt, S. W., Laskin, A., Nizkorodov, S. S., Eds.; ACS Symposium Series 1299; American Chemical Society: Washington, DC, 2018; pp 171−191.

(32) Craig, R. L.; Peterson, P. K.; Nandy, L.; Lei, Z.; Hossain, M. A.; Camarena, S.; Dodson, R. A.; Cook, R. D.; Dutcher, C. S.; Ault, A. P. Direct Determination of Aerosol pH: Size-Resolved Measurements of

DOI: 10.1021/acs.jpclett.9b00757
J. Phys. Chem. Lett. 2019, 10, 4476−4483

Submicrometer and Supermicrometer Aqueous Particles. *Anal. Chem.* **2018**, *90*, 11232−11239.
(33) Keene, W. C.; Pszenny, A. A. P.; Maben, J. R.; Sander, R. Variation of Marine Aerosol Acidity with Particle Size. *Geophys. Res. Lett.* **2002**, *29*, 5-1−5-4.
(34) Song, S.; Gao, M.; Xu, W.; Shao, J.; Shi, G.; Wang, S.; Wang, Y.; Sun, Y.; McElroy, M. B. Fine-Particle pH for Beijing Winter Haze as Inferred from Different Thermodynamic Equilibrium Models. *Atmos. Chem. Phys.* **2018**, *18*, 7423−7438.
(35) Colussi, A. J. Can the PH at the Air/Water Interface Be Different from the pH of Bulk Water? *Proc. Natl. Acad. Sci. U. S. A.* **2018**, *115*, E7887.
(36) Pilinis, C.; Capaldo, K. P.; Nenes, A.; Pandis, S. N. MADM-A New Multicomponent Aerosol Dynamics Model. *Aerosol Sci. Technol.* **2000**, *32*, 482−502.
(37) Wei, H.; Vejerano, E. P.; Leng, W.; Huang, Q.; Willner, M. R.; Marr, L. C.; Vikesland, P. J. Aerosol Microdroplets Exhibit a Stable pH Gradient. *Proc. Natl. Acad. Sci. U. S. A.* **2018**, *115*, 7272−7277.
(38) National Research Council. *Human Exposure Assessment for Airborne Pollutants*; National Academies Press: Washington, DC, 1991.
(39) Freedman, M. A.; Ott, E.-J. E.; Marak, K. E. Role of pH in Aerosol Processes and Measurement Challenges. *J. Phys. Chem. A* **2019**, *123*, 1275−1284.
(40) Koutrakis, P.; Thompson, K. M.; Wolfson, J. M.; Spengler, J. D.; Keeler, G. J.; Slater, J. L. Determination of Aerosol Strong Acidity Losses Due to Interactions of Collected Particles: Results from Laboratory and Field Studies. *Atmos. Environ., Part A* **1992**, *26*, 987−995.
(41) Dallemagne, M. A.; Huang, X. Y.; Eddingsaas, N. C. Variation in pH of Model Secondary Organic Aerosol during Liquid− Liquid Phase Separation. *J. Phys. Chem. A* **2016**, *120*, 2868−2876.
(42) Harris, D. C. *Quantitative Chemical Analysis*, 7th ed.; W.H. Freeman and Co: New York, 2010.
(43) Po, H. N.; Senozan, N. M. The Henderson-Hasselbalch Equation: Its History and Limitations. *J. Chem. Educ.* **2001**, *78*, 1499−1503.
(44) Radić, N.; Prkić, A. Historical Remarks on the Henderson-Hasselbalch Equation: Its Advantages and Limitations and a Novel Approach for Exact pH Calculation in Buffer Region. *Rev. Anal. Chem.* **2012**, *31*, 93−98.
(45) Levine, I. N. *Physical Chemistry*, 5th ed.; Boston: McGraw-Hill, 2002.
(46) Grenthe, I.; Mompean, F.; Spahiu, K.; Wanner, H. *TDB-2 Guidelines for the Extrapolation to Zero Ionic Strength*; OECD Nuclear Energy Agency: Issy-les-Moulineaux (France), 2013.
(47) Skoog, D. A.; West, D. M.; Holler, F. J. *Analytical Chemistry: An Introduction*, 6th ed.; Saunders College Publishing: Philadelphia, 1994.
(48) Sipos, P. Application of the Specific Ion Interaction Theory (SIT) for the Ionic Products of Aqueous Electrolyte Solutions of Very High Concentrations. *J. Mol. Liq.* **2008**, *143*, 13−16.
(49) Ciavatta, L. The Specific Interaction Theory in Evaluating Ionic Equilibria. *Ann. Chim. (Rome)* **1980**, 551−562.
(50) Guggenheim, E. A.; Turgeon, J. C. Specific Inteaction of Ions. *Trans. Faraday Soc.* **1955**, *51*, 747−761.
(51) Ekberg, C.; Brown, P. L. *Hydrolysis of Metal Ions*; Wiley-VCH: Germany, 2016.
(52) Yan, X.; Bain, R. M.; Cooks, R. G. Organic Reactions in Microdroplets: Reaction Acceleration Revealed by Mass Spectrometry. *Angew. Chem., Int. Ed.* **2016**, *55*, 12960−12972.
(53) *CRC Handbook of Chemistry and Physics*, 84th ed.; Lide, D. R., Ed.; CRC Press LLC: Boca Raton, FL, 2003.
(54) Mishra, H.; Enami, S.; Nielsen, R. J.; Stewart, L. A.; Hoffmann, M. R.; Goddard, W. A.; Colussi, A. J. Brønsted Basicity of the Air-Water Interface. *Proc. Natl. Acad. Sci. U. S. A.* **2012**, *109*, 18679−18683.
(55) Enami, S.; Hoffmann, M. R.; Colussi, A. J. Proton Availability at the Air/Water Interface. *J. Phys. Chem. Lett.* **2010**, *1*, 1599−1604.
(56) Zhao, X.; Subrahmanyan, S.; Eisenthal, K. B. Determination of pKa at the Air/Water Interface by Second Harmonic Generation. *Chem. Phys. Lett.* **1990**, *171*, 558−562.

DOI: 10.1021/acs.jpclett.9b00757
J. Phys. Chem. Lett. 2019, 10, 4476−4483